Templated Deposition of MoS_2 Nanotubules Using Single Source Precursor and Studies of Their Optical Limiting Properties

Kian Ping Loh,*,† Heng Zhang,† Wei Zhe Chen,‡ and Wei Ji*,‡

Department of Chemistry, National University of Singapore, 3 Science Drive 3, Singapore 117543, Department of Physics, National University of Singapore, 3 Science Drive 2, Singapore 117543

Received: October 18, 2005; In Final Form: November 30, 2005

We demonstrate a simple way of fabricating bulk quantities of molybdenum disulfide (MoS_2) porous nanotubules (NTs) by templated deposition from a single source precursor based on tetrakis(diethylaminodithiocarbomato)molybdate(IV). Bulk quantities of crystalline MoS_2 NTs that consist of agglomerates of nested nanocapsules were obtained by this one-step evaporation method. We found that MoS_2 NTs show good optical limiting behavior with 532-and 1064-nm nanosecond laser pulses, and the size-effect of the NTs on optical transmission was observed.

1. Introduction

Nanotubes[1] as well as nanoclusters of the layered metal disulfides, MoS_2 and WS_2, continue to generate considerable interest because of their potential applications in catalysis and electrochemical hydrogen storage. MoS_2 can be synthesized in a large variety of forms ranging from particles, nanotubes, nanosheets, and nanobelts to fullerenes.[2−5] The richness in form promises potential applications going beyond those of carbon nanotubes. Previous methods for the synthesis of the MoS_2 nanotubes (NTs) rely on the hydrogen reduction of the corresponding solid trisulfides or thiomolybate precursors.[2−8] For example, near-monodisperse, poorly crystalline MoS_2 NTs had been obtained by Dorhout[4] by the thermal reduction of ammonium thiomolybdate precursors within the confined voids of an alumina template in an atmosphere of H_2/N_2. The use of a single source solid precursor which can be evaporated in vacuum for the chemical vapor deposition (CVD) of MoS_2 nanotubes has not been reported, due mainly to the nonavailability of volatile MoS_2 precursors. CVD from a single source precursor offers advantages in terms of the ease of operation, compatibility with the lithographical process, and industrial scale-up; it also avoids the use of toxic hydrogen sulfide. In this paper, we report a new strategy for the growth of MoS_2 porous NTs by the thermal evaporation of tetrakis(diethylaminodithiocarbomato)-molybdate(IV)[8,9] on an anodized alumina template in high vacuum, at temperatures below 600 °C. Previously, we have demonstrated the versatility of this precursor for the deposition of crystalline MoS_2 nanosheets,[8] as well as MoS_2-derived solid-state diffusion-substitution films such as $MoSi_2$ and $MoGe_2$.[9] Here we report a method for the generation of large quantities of highly porous MoS_2 NTs from the single source precursor.

The optical limiting properties have not been investigated in the case of MoS_2. Optical limiters are devices that transmit light at low intensities but block light at high intensities, effectively keeping the amount of transmitted light below a certain level. The optical limiting (OL) properties of fullerenes,[10] metallophthalocyanines and porphyrins, carbon black,[12,13] carbon nanotubes,[14−18] semiconductor nanomaterials,[19,20] and metal nanoclusters[21,22] have been investigated extensively. One advantage of MoS_2 in terms of optical or photochemical application arises from its photostability because both its valence and conduction bands are composed primarily of nonbonding Mo 4*d* orbitals, resulting in very little bond extension and weakening upon photoexcitation. Another possibility is excited-state absorption or possible nonlinear scattering in the MoS_2 NTs, which makes them an ideal candidate for broadband optical limiting (OL) application, as demonstrated in the following.

2. Experimental Section

The procedures for the synthesis of the tetrakis(diethylaminodithiocarbomato)molybdate(IV) precursor have been reported previously by us.[8,9] The anodic alumina membrane (AAO) was synthesized following the standard two-step anodization process of Al foils in acid solutions. The size of the pores could be varied from 50 to 300 nm, depending on the anodization acid used or the anodization voltage. A Knudsen cell was used to evaporate the precursor (0.1 g) in a dynamic vacuum of 1×10^{-6} Torr onto an alumina template mounted on a 2-in. substrate heater. The evaporation temperature of the precursor was maintained at 300 °C, while the temperature of the AAO template was varied between 600 and 700 °C to control the decomposition rate of the precursors in the template. Increasing the temperature beyond 500 °C is necessary for the precursors to decompose completely into MoS_2 and release the rest of the moieties in the precursors, possibly as gaseous ethylene, ethylenediamine, hydrogen cyanide, and sulfur. The temperature of the template controls the kinetics of decomposition and MoS_2 formation within the pores; that is, a high template temperature resulted in the growth of solid nanofibers due to rapid hole filling, while a low template temperature resulted only in the coating of the walls of the pores, giving rise to porous nanofibers instead. In this work, we call the porous nanofibers "nanotubules (NTs)" to distinguish them from the crystalline nanotubes.

To compare the OL properties of MoS_2 NTs with carbon nanotubes, suspensions of MoS_2 NTs and multiwalled carbon nanotubes (MWCNTs) were prepared by sonicating the nanotubes in distilled water for 10 minutes. The concentration of both the NTs and MWCNT suspensions was adjusted to give a

* Corresponding authors. E-mail: chmlohkp@nus.edu.sg (K. P. Loh); phyjiwei@nus.edu.sg (W. Ji).
† Department of Chemistry.
‡ Department of Physics.

10.1021/jp055959t CCC: $33.50
Published on Web 12/31/2005

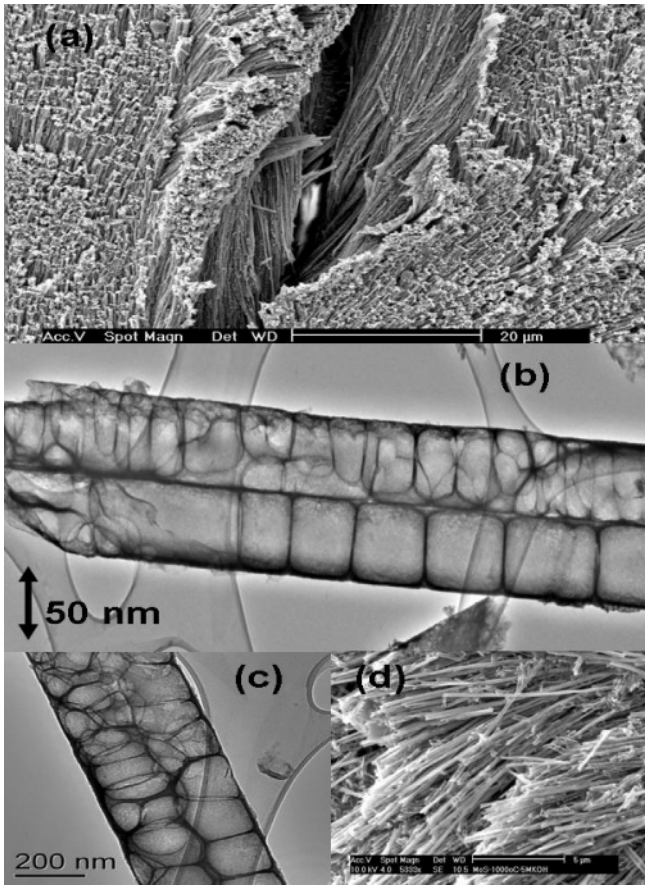

Figure 1. (a) and (d), SEM images of the MoS_2 nanotubules (NTs) grown on AAO template; (b) and (c), TEM images of the nanotubules.

linear transmission of ~65% at 532 nm in a 1-cm-thick quartz cell. Their linear transmission spectra were recorded with a spectrophotometer (Shimadzu PharmaSpec UV-1700) from 200 to 1100 nm.

3. Results and Discussion

Figure 1 shows densely packed, vertically erected MoS_2 NTs synthesized on the AAO template. Part of the AAO template has been dissolved away to expose the vertically erect NTs inside, as shown in the SEM image in Figure 1a. The dimensions of the MoS_2 NTs are defined by the size of pores in the AAO template; typically the diameter of the NTs can be varied between 50 and 300 nm, while the lengths are approximately 10 μm. Figure 1d shows the SEM images of NTs recovered from the alumina template and dispersed on a substrate. Figure 1b,c show the TEM images of individual NTs, where it can be seen that the NTs of ~100−200-nm diameter are highly porous and consist of multiple interlocked nanocapsules. The MoS_2 layers are curved along the transecting region to form segments. Such bamboo-like NTs with internal compartments separating the capsules had also been observed by Dorhout[4] in his templated synthesis of MoS_2 by the thermal decomposition of $(NH_4)_2MoS_4$. The similarity of the NTs obtained in their case, and ours, suggest that the decomposition of the precursors in the channeled-confined space in both cases generates a three-dimensional growth profile to form these nanocapsules in the NTs. The NTs (Figure 1d) can be recovered from the AAO template after dissolving the template. The powder X-ray diffraction (XRD) spectrum of the MoS_2 NTs is shown in Figure 2, where the strongest peaks can be assigned to the hexagonal phase (2H).[29] Some rhombohedral phase can be detected as well.

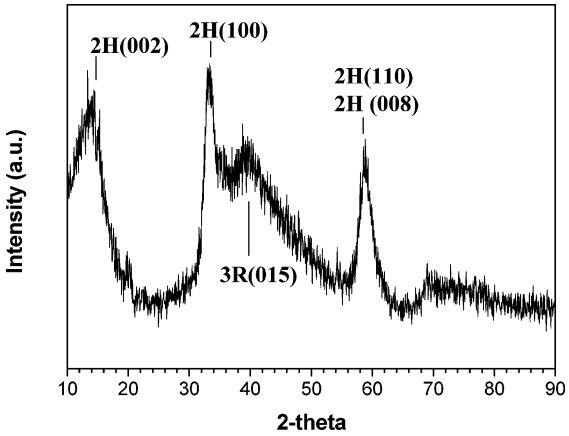

Figure 2. Powder XRD of the MoS_2 nanotubules.

The SEM images in Figure 3 show the sequences at the various stages of the recovery of the MoS_2 NTs from the AAO template following its dissolution. The free-standing AAO template which was evaporation-filled with MoS_2 NTs was transferred onto a flat substrate (for example, silicon), and a drop of alkali was introduced for the dissolution of the AAO template. After fixed time intervals of 8, 10, and 20 min, we rinsed the surface with deionized water, dried the sample, and observed it under SEM. The AAO template acted as an isolation matrix for the individual NTs; following its dissolution, electrostatic forces between the separated MoS_2 NTs can provide a driving force for the self-assembly on the substrate. Figure 3a shows vertical NTs which assembled together to form walls after 8 to 10 min of alkali dissolution. The alkali drop became saturated with the aluminate ions during the dissolution process, and some of these precipitated on-top of the vertical NTs. After 20 min of alkali dissolution, the NTs collapsed and lay parallel on the substrate, but some form of self-assembly into "fin-shape" patches can be seen. Essentially the surface of the silicon substrate can be covered with either standing NTs or flat-lying NTs that exhibited some form of self-assembly, depending on the dissolution time in the alkali.

Figure 4a shows the linear transmission spectra of MoS_2 NTs and MWCNTs. Similar to the previous reports,[14−18] the spectrum of MWCNTs is nearly flat in the visible range, while several absorption peaks can be seen in the spectra of MoS_2 NTs. The peaks between 600 and 700 nm are assigned to the two-exciton absorptions, which had been previously reported in bulk 2H-MoS_2.[23] The band-gap of MoS_2 is ~1.2 eV, associated with an indirect gap between the Γ and K point (Figure 4b). The *A* and *B* excitons are assigned to the direct transitions at the K point of the Brillouin zone, and the *A* and *B* splitting is due to interlayer interaction and spin−orbit splitting. Another peak at 400−500 nm may be related to a direct transition from deep states in the valence band to the conduction band.[24] Size effects are apparent; that is, the thinner MoS_2 NTs (50−100 nm) have stronger absorption than the thicker ones in the 300−400-nm range, while the thicker NTs (300−400 nm) have a stronger adsorption in the 800−1000-nm range. This may be due to surface resonance effects on the thinner NTs; optical adsorptions arising from either surface plasmon or surface state bands are stronger on nanomaterials with a higher surface-to-bulk ratio.

The optical limiting (OL) measurements were conducted with linear polarized laser pulses of 7-ns duration from frequency-doubled, Q-switched Nd:YAG laser. The spatial distribution of the pulses was nearly Gaussian after passing through a spatial filter. The pulses were divided by a beam splitter into two parts.

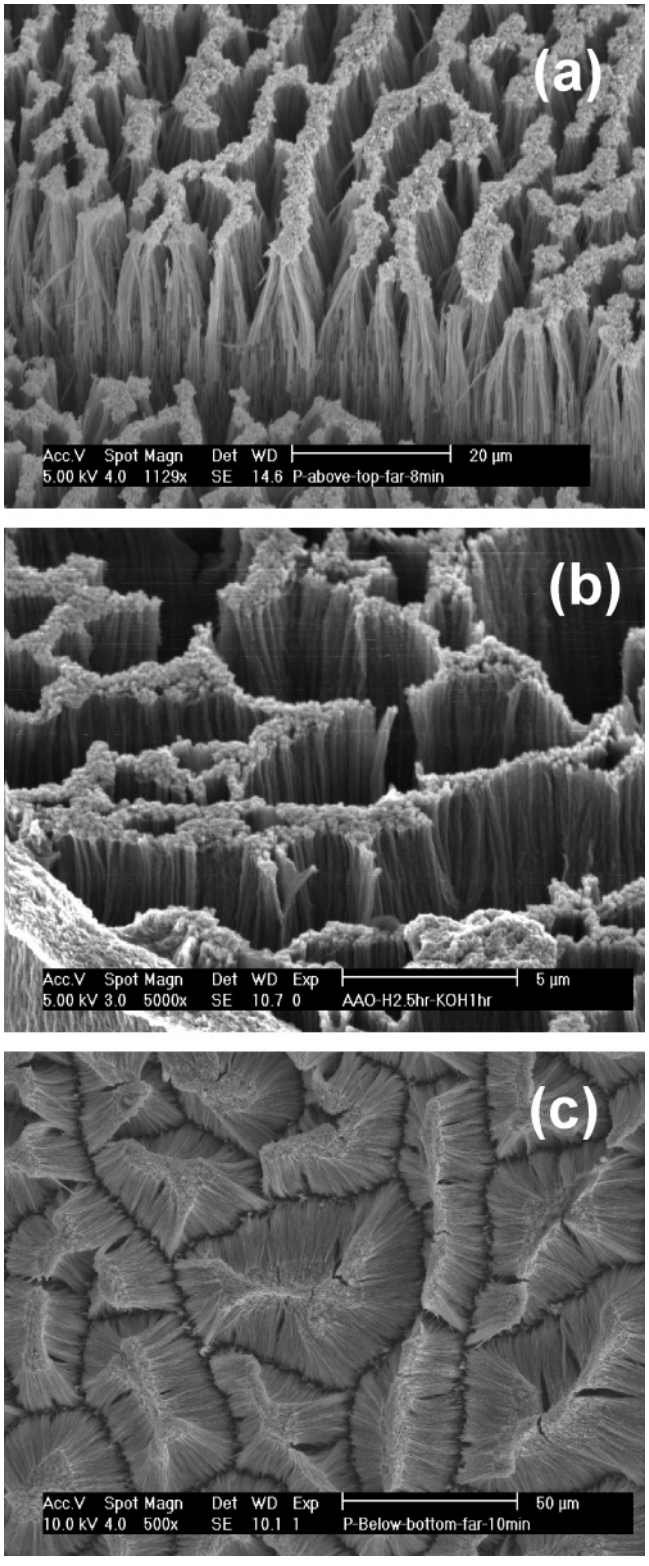

Figure 3. SEM images of the self-assembled structure formed by the MoS_2 NTs on silicon after dissolving the AAO template in a drop of alkali for (a) 8 min, (b) 12 min, and (c) 20 min. The free-standing AAO template was placed on a piece of silicon wafer.

The reflected part was taken as the reference representing the incident pulse energy, and the transmitted beam was focused through the sample. The sample was fixed at the focus. Both the incident and the transmitted pulse energies were measured simultaneously by two pyro-electric detectors (PjP-735). The beam waists of the focused laser beam were 40 and 80 μm at

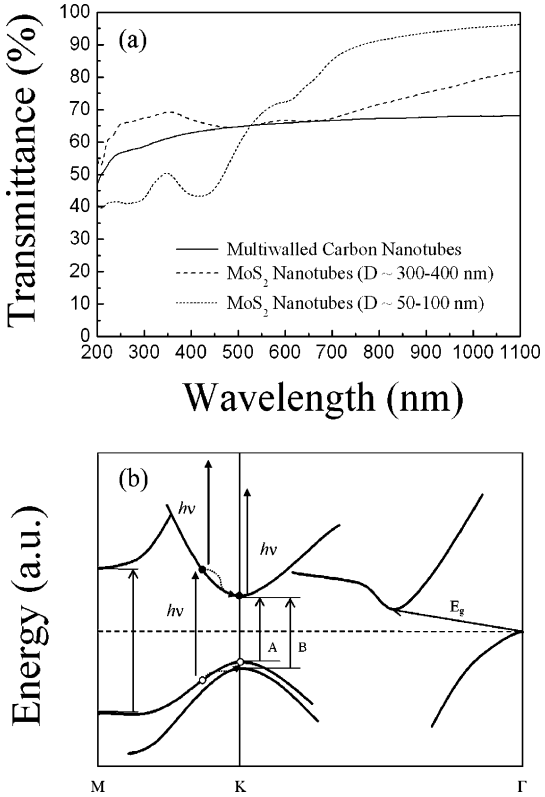

Figure 4. (a) Linear transmission spectra of MWCNTs and MoS_2 NTs with different diameters. (b) Schematic of the band structure of MoS_2 showing the various possible transitions. The band-to-band transition across the mimimum gap (E_g) is indicated by the angled arrow.

532 and 1064 nm, respectively, which was determined by the standard z-scan method.[25] The laser was operated at single shots or 10 Hz.

Figure 5a shows the OL behavior of MoS_2 NTs suspensions at 532 nm. Results of MWCNT suspensions recorded under the same conditions are also displayed for comparison. MoS_2 NTs clearly exhibit stronger OL compared to MWCNTs, especially for the smaller-diameter NTs. At an incident fluence of 4.0 J/cm^2, the decrease in the transmittance is observed to be 13% more for the thinner MoS_2 NTs, compared with MWCNTs. Furthermore, we note that MoS_2 NTs show the size dependence of OL behavior, with the thin MoS_2 NTs performing better than the thick ones. Figure 5b demonstrates that MoS_2 NTs are also a broadband limiter with wavelengths of up to 1064 nm and have OL capability similar to that of MWCNTs at 1064-nm wavelength. To quantitatively describe the limiting behavior, we define the limiting threshold, F_{th}, as the input fluence at which the transmittance falls to 50% of the linear transmittance. Table 1 summarizes the measured limiting thresholds.

To identify the OL mechanism of MoS_2 NTs, the angular dependence of the forward nonlinear scattering measurement was carried out. When the sample was irradiated by 7-ns laser pulses at normal incidence, the forward scattered energy was recorded at forward angles from 10° to 80° in steps of 10° with a solid angle ~0.015 steradian by a high-resolution pyro-electric detector. Since nonlinear scattering has been established as the OL mechanism of MWCNT suspensions,[13−18,26] a MWCNT sample was used for comparison. The forward-scattering results of MoS_2 NTs with different diameters at 532 nm are illustrated in Figure 6, showing that the forward-scattered light in both MoS_2 NTs and MWCNTs is increased significantly as the input fluence increases. The similar scattering results indicate that nonlinear scattering is the dominant mechanism for the OL

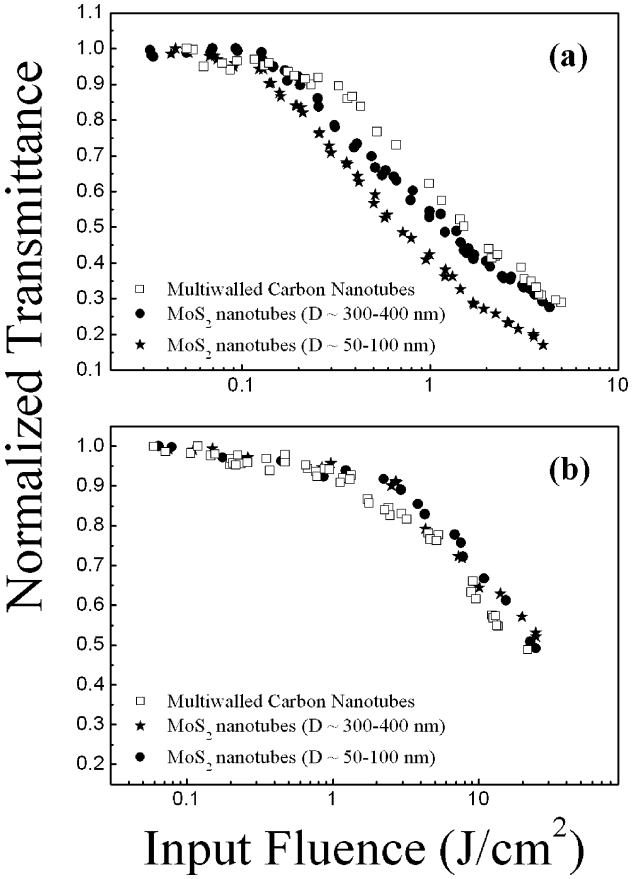

Figure 5. Optical limiting of MoS_2 NTs with different diameters suspended in water measured by 7-ns laser pulses at (a) 532 nm and (b) 1064 nm. A MWCNTs sample was used as a reference in both conditions. The linear transmittance of all the samples was adjusted to about 65% at 532 nm and 90% at 1064 nm, respectively.

TABLE 1: Limiting Thresholds, F_{th}, Measured with Nanosecond Laser Pulses at 532 and 1064 nm

samples	F_{th} at 532 nm (J/cm^2)	F_{th} at 1064 nm (J/cm^2)
multiwalled carbon nanotubes	1.3	20
MoS_2 NTs (diameter ~ 300−400 nm)	1.1	22
MoS_2 NTs (diameter ~ 50−100 nm)	0.7	22

behavior of MoS_2 NTs. During laser irradiation over a critical fluence, MoS_2 NTs became heated, and they acted as initial centers for solvent bubble growth while dissipating the thermal energy to the surrounding solution. As the input fluence was increased further, sublimation of the MoS_2 NTs could occur to form micrometer-sized plasma. The nonlinear scattering from bubbles and micro-plasmas provides the strong OL responses.

Although nonlinear scattering is the main OL mechanism, nonlinear absorption cannot be excluded from the OL effect at 532 nm for MoS_2 NTs. The MoS_2 NTs exhibit much stronger OL properties than MWCNTs; therefore, the free-carrier absorption (FCA) may have a role in influencing the OL behavior. Since the photon energy of 532-nm laser pulses is higher than the lowest direct band gap, absorption of an incident photon promotes an electron to the conduction band to form a free carrier, simultaneously producing a hole. The FCA process involves the absorption by the electron of another photon, and being promoted to a higher state in the conduction band. The FCA process can lead to the reduction of transmittance when the incident fluence increases, which has been reported in

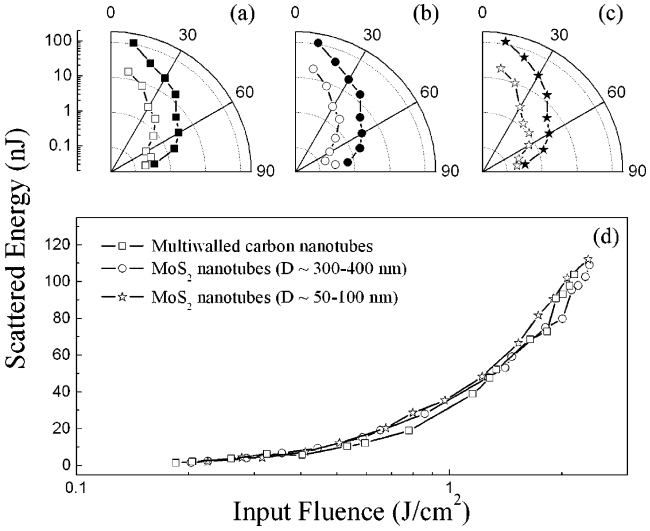

Figure 6. Angular dependence of nonlinear scattering measurement at 532 nm. (a) MWCNTs with $F_i \sim 0.7$ J/cm^2 (open square) and $F_i \sim 2.3$ J/cm^2 (solid square); (b) MoS_2 NTs ($D \sim 300-400$ nm) with $F_i \sim 0.7$ J/cm^2 (open circle) and $F_i \sim 2.3$ J/cm^2 (solid circle); (c) MoS_2 NTs ($D \sim 50-100$ nm) with $F_i \sim 0.7$ J/cm^2 (open star) and $F_i \sim 2.3$ J/cm^2 (solid star); (d) scattering of all the three samples with 10° forward angle at different incident fluences.

semiconductor materials such as $Cd_xAg_{1-x}S$ nanoparticles[19] and crystalline Si.[27]

4. Conclusions

We have fabricated bulk quantities of MoS_2 nanotubules (NTs) by the chemical vapor deposition of a single source precursor based on tetrakis(diethylaminodithiocarbomato)-molybdate(IV). This is a direct one-step vacuum evaporation process without the need for hydrogen reduction process. The optical limiting response of the MoS_2 NTs suspended in water has been observed with nanosecond laser pulses. MoS_2 NTs exhibit a lower limiting threshold value of 1.0 J/cm^2 compared to 1.3 J/cm^2 for multiwalled carbon nanotubes at 532 nm nanosecond pulse; the explanation may be due to the excited-state adsorption mechanism in the MoS_2 NTs.

Acknowledgment. K.P.L. and Z.H. acknowledge the support of NUSNNI as well as NUS Research Grant No. R-143-000-221-112 for this work.

References and Notes

(1) Tenne, R.; Margulius, L.; Genut, M.; Hodes, G. *Nature* **1992**, *360*, 444.
(2) Nath, M.; Rao, C. N. R. *J. Am. Chem. Soc.* **2001**, *123*, 4841.
(3) Nath, M.; Govindaraj, A.; Rao, C. N. R. *Adv. Mater.* **2001**, *13*, 283.
(4) Zelenski, C. M.; Dorhout, P. K. *J. Am. Chem. Soc.* **1998**, *120*, 743.
(5) Rapoport, L.; Bibik, Y.; Feldman, Y.; Homyonfer, M.; Cohen, S. R.; Tenne, R. *Nature* **1997**, *387*, 791.
(6) Chen, J.; Li, S. L.; Xu, Q.; Tanaka, K. *Chem. Commun.* **2002**, *20*, *1722*.
(7) Chen, J.; Li, S. L.; Tao, Z. L. *J. Alloys Compd.* **2003**, *356*, 413.
(8) Zhang, H.; Loh, K. P.; Sow, C. H.; Gu, H.; Su, X. *Langmuir* **2004**, *20*, 6914.
(9) Ouyang, T.; Loh, K. P.; Zhang, H.; Vittal, J. J.; Wee, A. T. S. *J. Phys. Chem. B* **2004**, *108*, 17537.
(10) Tutt, L. W.; Kost, A. *Nature* **1992**, *356*, 225.
(11) Perry, J. W.; Mansour, K.; Lee, I. S. Y.; Wu, X. L.; Bedworth, P. V.; Chen, C. T.; Marder, S.; Miles, P. *Science* **1996**, *273*, 1533.
(12) Mansour, K.; Soileau, M. J.; Van Stryland, E. W. *J. Opt. Soc. Am.* **1992**, *B9*, 1100.
(13) Sun, X.; Yu, R. Q.; Xu, G. Q.; Hor, T. S. A.; Ji, W. *Appl. Phys. Lett.* **1998**, *73*, 3632.
(14) Chen, P.; Wu, X.; Sun, X.; Lin, J.; Ji, W.; Tan, K. L. *Phys. Rev. Lett.* **1999**, *82*, 2548.

(15) Vivien, L.; Anglaret, E.; Riehl, D.; Bacou, F.; Journet, C.; Goze, C.; Andrieux, M. *Chem. Phys. Lett.* **1999**, *307*, 317.
(16) Riggs, J. E.; Walker, D. B.; Carroll, D. L.; Sun, Y. P. *J. Phys. Chem. B* **2000**, *104*, 7071.
(17) O'Flaherty, S. M.; Murphy, R.; Hold, S. V.; Cadek, M.; Coleman, J. N.; Blau, W. J. *J. Phys. Chem. B* **2003**, *107*, 958.
(18) Xu, J. F.; Czerw, R.; Webster, S.; Carroll, D. L.; Ballato, J.; Nesper, R. *Appl. Phys. Lett.* **2002**, *81*, 1711.
(19) Jia, W.; Douglas, E. P.; Guo, F.; Sun, W. *Appl. Phys. Lett.* **2004**, *85*, 6326.
(20) Francois, L.; Mostafavi, M.; Belloni, J.; Delouis, J. F.; Delaire, J.; Feneyrou, P. *J. Phys. Chem. B* **2000**, *104*, 6133.
(21) Philip, R.; Ravindra, G.; Sandhyarani, K. N.; Pradeep, T. *Phys. Rev. B* **2000**, *62*, 13160.
(22) Tenne, R.; Margulis, L.; Genut, M.; Hodes, G. *Nature* **1992**, *360*, 444.
(23) Frey, G. L.; Elani, S.; Homyonfer, M.; Feldman, Y.; Tenne, R. *Phys. Rev. B* **1998**, *57*, 6666.
(24) Wilcoxon, J. P.; Newcomer, P. P.; Samara, G. A. *J. Appl. Phys.* **1997**, *81*, 7934.
(25) Sheik-Bahae, M.; Said, A. A.; Wei, T.; Hagan, D. J.; Van Stryland, E. W. *IEEE J. Quantum Electron.* **1990**, *26*, 760.
(26) Sun, X.; Xiong, Y. N.; Chen, P.; Lin, J.; Ji, W.; Lim, J. H.; Yang, S. S.; Hagan, D. J.; Stryland, W. W. V. *Appl. Opt.* **2000**, *39*, 1998.
(27) Boggess, T. F.; Bohnert, K.; Mansour, K.; Moss, S. C.; Boyd, I. W.; Smirl, A. L. *IEEE J. Quantum Electron.* **1986**, *22*, 360.
(28) Cheon, J.; Gozum, J. E.; Girolami, G. S. *Chem. Mater.* **1997**, *9*, 1847.